Use of multiple lines of evidence to understand reactive mercury concentrations and chemistry in Hawai'i, Nevada, Maryland, and Utah, USA

3 4

1

2

- 5 Adriel Luippold¹, Mae Sexauer Gustin^{1*}, Sarrah M. Dunham-Cheatham¹, Mark Castro²,
- 6 Winston Luke³, Seth Lyman⁴, Lei Zhang⁵

7

- 8 ¹ Department of Natural Resources and Environmental Science, University of Nevada, Reno,
- 9 NV 89557, USA
- ² Appalachian Laboratory, University of Maryland Center for Environmental Science,
- 11 Frostburg, MD 21532, USA
- ³ Air Resources Laboratory, National Oceanic and Atmospheric Administration, College
- 13 Park, MD 20740, USA
- ⁴ Bingham Research Center, Utah State University, Vernal, UT 84322, USA
- ⁵ School of the Environment, Nanjing University, Nanjing, Jiangsu 210023, China

16 17

*Corresponding author: Mae Sexauer Gustin, mgustin@cabnr.unr.edu, 001-775-784-4203

18 19

Abstract

- 20 To advance our understanding of the mercury (Hg) biogeochemical cycle, concentrations
- 21 and chemistry of gaseous oxidized Hg (GOM), particulate bound Hg (PBM) and reactive Hg
- 22 (RM = GOM + PBM) need to be known. The UNR-RMAS 2.0 provides a solution that will
- advance knowledge. From 11/2017 to 02/2019, the RMAS 2.0 was deployed in Hawai'i,
- Nevada, Maryland, and Utah to test system performance and develop an understanding of
- 25 RM at locations impacted by different atmospheric oxidants. Mauna Loa Observatory,
- 26 Hawai'i, impacted by the free troposphere and the marine boundary layer, had primarily -
- 27 Br/Cl RM compounds. The Nevada location, directly adjacent to a major interstate highway
- and experiences inputs from the free troposphere, exhibited -Br/Cl, -N, -S, and organic
- compounds. In Maryland, compounds observed were -N, -S, and organic Hg. This site is
- downwind of coal fired power plants and located in a forested area. The location in Utah is
- in a basin impacted by oil and natural gas extraction, multiday wintertime inversion
- episodes, and inputs from the free troposphere. Compounds were -Br/Cl or -0, -N, and -
- 33 Br/Cl. The chemical forms of RM identified were consistent with the air source areas,
- 34 predominant ion chemistry, criteria air pollutants, and meteorology.

35

36 37

Keywords

- 38 gaseous oxidized mercury, thermal desorption, UNR-RMAS, cation exchange membrane,
- 39 back trajectory, ion chromatography

Graphical Abstract

Introduction

Atmospheric mercury (Hg) chemistry is a poorly understood component of the Hg biogeochemical cycle. Gaseous elemental Hg (GEM) in the atmosphere is oxidized to form gaseous oxidized Hg (GOM). Both can interact with aerosols to form particulate bound Hg (PBM)¹. GEM can be deposited to and re-emitted from surfaces (e.g. Miller and Gustin²). GOM can be deposited to surfaces and emitted back to the air as GEM³. Since oxidation reactions can occur quickly and deposited GEM and GOM can be re-emitted, the lifetime of of gaseous Hg in the atmosphere may be as short as a few hours³. While in the free troposphere/stratosphere the lifetime is on the order of 4 to 12 months.

Currently the only commercially available instrument for measurement of the 3 forms of atmospheric Hg is the automated Tekran® 2537/1130/1135. The instrument components collect GEM, GOM, and PBM, respectively. The KCl-coated denuder used to collect GOM has been shown to underestimate concentrations by up to 13 times³⁻⁷. There are artefacts associated with the PBM measurement, and the 1135 unit has been shown to collect GOM^{5,8}. Because of the limitations of this instrument, this research focused on using a membrane-based system for the collection of reactive Hg (RM = GOM + PBM) compounds to quantify total RM concentrations, as well as identify RM compounds present in ambient air at field sites with different atmospheric chemistry. The University of Nevada, Reno-Reactive Mercury Active System (UNR-RMAS) has been a technology in the making for over 10 years and has been deployed at sites in Nevada⁹⁻¹¹, Florida¹², Australia, and Tasmania¹³ (see Graphical Abstract). The UNR-RMAS 2.0¹⁴ was used in this study at locations in

Hawai'i, Nevada, Maryland, and Utah. In 2019, it was also deployed at Svalbard, Norway and in Nanjing, China. The RMAS 2.0 uses cation exchange membranes (CEM) to quantify RM concentrations and nylon membranes to identify RM chemistry^{5,14}. CEM are digested and analyzed for RM concentrations. Nylon membranes are thermally desorbed to determine the chemistry of the RM compounds on the membrane. For additional information on improvements to the RMAS system see the Supplemental Information (SI) and Luippold et al. (2020)¹⁴.

The RMAS 2.0 has a few known limitations, including needing to be deployed for 3 days to 2 weeks. In addition, better understanding of limitations of the membranes as collection surfaces is needed, though recent work has increased confidence in the CEM ability to quantify RM. For example, a paper recently submitted by Lyman et al. 15 compared concentrations measured using a calibrated dual channel system that quantified GEM by scrubbing air of RM using a CEM, and measured total gaseous Hg (TGM) by pulling air through a pyrolyzer allowing for calculation of RM (RM = TGM - GEM). When the RMAS 2.0 collected data alongside the dual channel system, RMAS 2.0 CEM average values were the same as the dual channel system (34 ± 5 versus 36 ± 13 pg m $^{-3}$, respectively). The dual channel system was calibrated using permeated HgCl2 and HgBr2.

In this research the utility of the RMAS 2.0 as a RM measurement method was investigated. CEM and nylon membrane RM concentrations and chemistry for each deployment period were compared with meteorology and criteria air pollutant data from the field sites. Potential sources of RM compounds were determined using back trajectory analyses. Ion chromatography was used to determine anion chemistry on membranes.

Given previous observations and the improved RMAS system, research hypotheses included: 1) the RMAS 2.0 will collect more RM than the Tekran® system, but this will vary depending on the chemistry of the RM compounds; 2) breakthrough observed could be impacted by artefacts or RM chemistry. 3) understanding breakthrough associated with the membranes will allow for developing a better understanding of what membranes capture; and 4) comparison of nylon and CEM concentrations will provide a framework for better understanding of RM chemistry and differences can be explained based on the dominant RM forms present. To address these research hypotheses a year of RM and ancillary data were collected for 4 field sites. Specific thermal desorption profiles from each site were compared with corresponding back trajectories, anion chemistry, and ancillary data. The percentage of different RM compounds present is also evaluated.

Methods

Field sites

The National Oceanic and Atmospheric Administration (NOAA) Moana Loa Observatory (MLO) is on the island of Hawai'i (19.5392, -155.5792; 3397 masl). This site is far from major sources of pollution and an optimal air sampling location in the free troposphere¹⁵ (www.esrl.noaa.gov/gmd/obop/mlo/). NOAA operates a Tekran® 1130/1135/2537 speciation system as a part of the AMNet network (2010 to present) (see Graphical Abstract). Deployment began February 7, 2018 and ended March 6, 2019, with membranes collecting RM for 2 weeks (n = 27).

The location in Reno, NV (39.5375, -119.8047; 1371 masl) was at the College of Agriculture, Biotechnology, and Natural Resources Agricultural Experiment Station Valley

Road Greenhouse Complex (GH). Membranes were deployed for two weeks from March 15, 2018 until July 17, 2018, and from then on for one week until March 12, 2019 (n = 42). The GH site is heavily influenced by road sources due to proximity to I-80, a major US interstate highway. This location hosted the UNR-RMAS in the past^{7,9}, and during this project a Tekran 2537/1130 system.

The Piney Reservoir site (MD) is north of Frostburg, Maryland (39.7053, -79.0122; 769 masl) located near the Maryland-Pennsylvania border, and is downwind of coal-fired power plants in Ohio, Pennsylvania, and West Virginia. Deployments at this location were for 2 weeks and spanned from December 20, 2017 to November 12, 2018 (n = 18). Previous studies at this field site indicated it has elevated GOM concentrations due to direct impact by local power plant sources from the west¹⁶⁻¹⁸. This site operated a Tekran® 1130/1135/2537 speciation system under AMNet (2008 to present).

Horsepool Monitoring Station, Utah (UT) (40.1434, -109.4689; 1567 masl) is in the Uintah Basin south of Vernal and Dinosaur National Monument. This area has significant oil and natural gas activity. The basin sometimes has persistent, multiday winter inversion episodes and high ozone¹⁹ that may impact oxidation chemistry of the Hg collected on the membranes. Deployments here were for 2 weeks and spanned from November 21, 2017 until February 27. 2019 (n = 27).

Details on the membranes, deployment, % breakthrough calculations, and thermal desorption are described in the SI. All dates presented hereafter represent the end date of the sampling period.

Peak deconvolution of thermal desorption profiles

A quantification method was developed to deconvolute and define individual GOM compound peaks from the thermal desorption profiles of field samples^{5, 14}. Based on the pure standard compounds and calibration of exact desorption temperature¹⁴, GOM compounds peak in the following ranges: 80–85 °C for [-0], 90–110 °C for [-Br/Cl], 125–135 °C for [-N], 150–155 °C for [-S], and 180–190 °C for methylmercury (MeHg) or organic-bound compounds. Note there are time periods when multiple overlapping compounds were found. The exact chemistry of the compounds is unknown; a method is needed to identify RM compounds other than the standard thermal desorption profiles already established and used to deconvoluted the thermal desorption profiles in this study. By comparing field sample desorption profiles to the profiles generated using pure compounds, the profile peaks from the field sample were assigned compound types. For peak deconvolution method details, see the SI. Fine particles will be collected on the filters given the system flow rate, because of this we are currently working on a system to separate GOM and PBM.

Tekran® speciation system

Tekran® systems were maintained and data processed following AMNet protocols

(http://nadp.slh.wisc.edu/lib/manuals/AMNet-2003 Operations Manual v 3-0.pdf). Data

collected that did not meet AMNet A or B quality standards was omitted from this study.

For details on the position of the inlets see the SI.

Ion chromatography

Anions on nylon membranes were determined using ion chromatography (IC), providing a framework for the assessment of whether identified RM compounds (i.e., by thermal desorption) were similar to major anions thought to be present in the air. For more details on the ion chromatography method, see the SI.

Back trajectories

The Hybrid Single-Particle Lagrangian Integrated Trajectory model (HYSPLIT), developed by NOAA Air Resources Laboratory^{20, 21} was used to calculate 240 h back trajectory simulations (GDAS 1° archive). Trajectories were created throughout the membrane sampling periods and then analyzed using the gridded frequency distribution method. For details and selected modeling parameters, see the SI text and Table SI 2.

Ancillary data and statistical analyses

Sources of ancillary data are presented in SI Table 3. Details of regression analyses are in the SI. Maps were made using ArcMap 10.6.1.

3. Results and discussion by site

163 3.1 MLO

At MLO RM concentration on the CEM and nylon membrane was 133 ± 5 pg m⁻³ (mean \pm standard deviation) and 77 ± 5 pg m⁻³, respectively, for the entire sampling campaign. During this time, the Tekran[®] system collected 82 ± 38 pg m⁻³ RM. RM concentrations were highest at MLO compared to the other sampling locations (Figure 1a).

Mean breakthrough for CEM was $5.0 \pm 1.0\%$, and $1.2 \pm 0.3\%$ for nylon membranes. It is noteworthy that at MLO there were 2 time periods when the CEM and Tekran® RM concentrations were not statistically significantly different, and two in which the overlap was close. Looking at temperature, and relative and absolute humidity across the time period there was nothing unique about this time period (data not shown).

There were two common thermal desorption profile shapes observed at MLO. Most (89%) had a single bell-shaped peak in the -Br/Cl range (Figure 2 MLO a). The profile shown in Figure 2a was dominated by -Br/Cl compounds based on peak deconvolution, with 74% of the RM desorbing the in the -Br/Cl temperature range of 90-110 °C. Ten-day back trajectory analyses for this sample indicated that air moved to MLO over the Pacific Ocean, and >25% of this air resided within the marine boundary layer (Figure 3: brown grids). The percentage of the points within 100 km of the site was 3%. All the profiles obtained at MLO for the entire sampling campaign can be found in the Figure SI 1.

The second thermal desorption profile shape at MLO was bimodal, with peaks in the -Br/Cl range and in the -N range. N peaks were only detected at MLO after the 2018 Kilauea eruption began. These samples (n = 3) were collected on 04/06/18 18/06/18, and 30/07/18 2018. The desorption profile for June 18th (Figure 2 MLO b) included 78% -N, 12% -Br/Cl, and 10% -S. Back trajectories for this deployment showed air came to MLO from over the Pacific Ocean then up from the south over the Kilauea eruption. Many of these trajectories resided beneath the marine boundary layer (Figure 3 b, brown), indicating a mix of influences from the free troposphere and within the marine boundary

layer from the direction of Kilauea, with contributed air within 100 km being 4%. For additional profiles with ion chemistry and back trajectories for MLO see Figure SI 4. All ion chemistry is presented in Table SI 3.

The Kilauea eruption from 04/05 to 04/08/18 was the largest lower East Rift Zone eruption and caldera collapse in 200 years²². GEM concentrations at MLO during this period were not significantly correlated with criteria air pollutants (p = 0.96; Table SI 4). Selected air pollutants, RM, and GEM measurements during the time period of the eruption are plotted in Figure SI 3. Sulfur dioxide (SO₂) concentrations increased after the eruption as did RM concentrations; however, O₃, relative humidity, and GEM showed no trends. RM chemistry and ancillary criteria air pollutant data suggest that the eruption may have influenced the chemistry of the compounds present; however, we do not have enough data to understand this.

RM, particularly -Br/Cl compounds, were likely formed from ocean and free tropospheric influences. Lin et al. 23 found increased O_3 precursor emissions (NO $_x$ and hydrocarbons) from Eurasia caused elevated autumn O_3 concentrations at MLO from 1996 – 2011 relative to the previous decade (1980 - 1995). Observations were coupled with models and CO tracers that indicated increased airflow from the west to MLO during the fall 23 . Thermal desorption profiles from 08/18-11/18 had pronounced -Br/Cl peaks with no secondary or widened peaks in the -N range. O_3 for this time were < 40 ppb and not elevated relative to the rest of the sampling campaign. MLO 10-day back trajectories (Figure SI 2) did not reside in the Eurasian source boxes for significant times. These trends indicate that the RM compounds on the membranes were not likely influenced by Eurasian

oxidants. For discussion of correlations between membrane concentrations, Tekran data, and ancillary data for all sites please see the SI.

Nylon membrane RM concentrations were always lower than CEM concentrations at MLO (Figure 1a). However, there was variation in the difference with the nylon membranes being 10% to 87% lower than the CEM. The largest differences in concentrations occurred from August through October, when nylon membrane RM concentrations were 30% to 87% lower than CEM. There were no significant correlations between % difference values (Equation 1) and the ancillary data (p > 0.05).

MLO nylon membranes analyzed for anions by IC (n = 9) identified SO_4^{2-} that ranged from 11 to 100% of all anions detected. The next most prevalent anion measured was chloride (Cl-), at 9-64% (Table SI 3). The presence of Cl- supports the profile peak deconvolution results of -Br/Cl compounds in corresponding thermal desorption profiles. Although SO_4^{2-} was measured on the membranes, Hg-S compounds were not present in the thermal desorption profiles. It is possible that RM compounds were not generated by oxidation associated with S compounds. HgSO₄ is typically generated from heterogeneous oxidation^{24,25}. Both S and Cl would be emitted from the ocean.

Another high elevation study by Marusczak et al. 26 , using a polyethersulfone cation exchange membrane and a Tekran system, was done at the Pic du Midi Observatory for 6 months. In this work the authors measured concentrations of RM of 198 ± 57 and 229 ± 58 pg m⁻³ in dry free troposphere air. Given that the Hg compounds were likely Br based and the air was dry, the denuder was likely working efficiently. During our study, RM concentrations measured by the Tekran at MLO did reach these values when the volcanic

eruption was occurring. Otherwise, values were lower and thermal desorption profiles indicated that compounds were primarily -Br and -Cl based. Case studies demonstrated a significant component of the sampled air was derived from the marine boundary layer; this is supported in this study by RH being > 35% most of the time (see excel file in the SI). Marusczak et al. 26 also suggested that adding the flush data from the Tekran® improved the agreement with their membranes. At MLO the average flush concentrations were provided by NOAA, and using these data the concentrations obtained were 1.9 ± 0.1 % of the total GOM measured. This in some cases would improve the comparison and others not make much of a difference. The correlation between the Tekran and CEM data for this location was $r^2 = 0.23$ and p = 0.01 (Table SI 4), indicating a significant, butpoor correlation. 3.2 GH

Mean RM concentration on the CEM at GH was 60 ± 40 pg m⁻³ and on the nylon membranes was 44 ± 3 pg m⁻³ (Figure 1b). The Tekran® system was offline much of 2018. While operating mean RM concentrations were 5 ± 4 pg m⁻³ and concentrations may be underestimated for the 1135 unit not used. When the Tekran® was online, CEM RM concentrations were 3.3- to 9.7-times higher than those measured by the Tekran®. This is within the range of 1.7- to 13-times reported by Gustin et al.9 for the same location and agrees with past comparisons^{3,7}. Mean percent breakthrough was $13 \pm 1\%$ for CEM and $7 \pm 2\%$ for nylon membranes.

Profiles at the GH were composed of -O, -Br/Cl, -N, -S, and organic-Hg compounds (Figure 2). These were similar to those reported in Gustin et al. ⁵ and Luippold et al. ¹⁴. The former applied a polytetrafluoroethylene PTFE membrane in front of a CEM with the goal of differentiating PBM versus GOM. At this location, GOM constituted 48 to 78% of RM and

PBM 22 to 52%. Gustin et al.⁵ pointed out that the profiles indicated a mixture of compounds, i.e. peaks between 88 to 92 °C could be HgBrOH or HgClOH; 115 to 120 °C - HgBrNO₃ or HgClNO₃; and those between 140 to 145 °C could be O₃–Hg–SO₄–Hg–NO₃ or other unidentified compounds. Mean breakthrough on the nylon membranes for this deployment was 0.7%, low relative to other nylon membranes from GH (see excel file in the SI). HYSPLIT trajectories for profile 3a showed that the GH site was influenced by long-range transport over the Pacific Ocean. Of the calculated trajectories, 0.02% resided in the Northern Eurasian source box, 0.01% in the East Asia source box, 0.11% in the San Francisco, California source box, and 8.8% within 100 km. The gridded frequency distribution showed that trajectories were concentrated over the Pacific Ocean from the west (yellow: 5-25% of trajectories; Figure 3). These trajectory patterns for transport to GH were similar to those reported in Pierce et al.¹¹.

For the deployment ending on 25/09/18 (Figure 3 GH b), the thermal desorption profile peaked in the -Br/Cl range and had a secondary peak in the -S range. The total residence time for trajectory points within the Northern Eurasia source box and East Asian source box was 0.2%. The frequency distributions indicated that air traveled over East Asia (Figure 3 GH b), then over the Pacific Ocean to the GH site in Nevada with 4.3% of the trajectory points within 100 km of the site It is possible the -S was derived from the marine boundary layer or from Asian sources as described in VanCuren and Gustin²⁷.

Profile Figure 2 GH c has very low concentrations and contained -O, -Br/Cl/N, -S, and organic-Hg compounds. The dominant peak was between the -Br/Cl and -N temperature ranges. Trajectories demonstrated a similar pattern to the previously

discussed GH samples (Figure 3) with 6.2% of the trajectory points residing in the Northern Eurasian source box, 1.71% in the East Asian source box, 2.1% in the San Francisco source box, and 4.6% within 100 km of the site. These trajectories were similar to those reported in Pierce et al.¹¹. Trajectories in brown grids indicated 25% probability of residence in the marine boundary layer. High elevation air parcels moved from Eurasia and dropped into the marine boundary layer before arriving at the GH site. Percent breakthrough of this sample (10%) was higher than for the samples GH a and b, and total RM on this nylon membrane was lower, indicating the possibility that the membrane did not collect RM chemistry associated with -N as effectively as the other cases where -Br/Cl was dominant. This supports the hypothesis that the nylon membranes collect compounds with varying efficiencies in ambient air. Additional trajectories with ion chemistry are in SI Figure SI 4. Additional trajectories are in Figure SI 5 and all GH profiles are in Figure SI 6.

At the GH, the first instance of nylon concentrations exceeding CEM concentrations was observed (c.f. $^{9,\,11-13}$). Nylon membrane RM concentrations at the GH site ranged from 90% lower to 23% higher than the CEM (Figure 1). During July through September, 2018, nylon membrane concentrations exceeded CEM concentrations by 5-23%, the maximum measurements for temperature (26.9 °C) and O_3 (73 ppb) were observed, along with higher solar radiation than in other seasons (> 240 Watts m $^{-2}$). It is thought if O_3 directly formed HgO this would make an aerosol that could be rapidly deposited; however, Hg oxide forms measured at the GH were measured as both GOM and PBM using the PTFE and CEM system 5 .

3.3 MD

Ion chromatography results for the GH (n=15) showed presence of SO_4^{2-} in all samples (Table SI 3). Cl⁻ was present in all samples analyzed except two, and the presence of Cl⁻ supports the observations of Br/Cl in GH samples. For Figure 3 GH b, the anion concentrations were 93% SO_4^{2-} and 7% Cl⁻ ions that coincided with the compounds found on peak deconvolution results for this profile: 48% Br/Cl/N and 28% S. An additional profile with this pattern is shown in Figure SI 4 (sample 5). Anions detected in these samples match the compounds desorbed from the membrane.

Mean RM concentration for samples collected at MD was 17 ± 2 pg m⁻³ for CEM with a mean breakthrough of $14 \pm 7\%$. For nylon membranes, the mean RM concentration was 6 ± 2 pg m⁻³ with a breakthrough of $8 \pm 3\%$. This site had the lowest total RM concentrations on membranes. There were 2 common profiles at this location (Figure 2 and Figure SI 4 samples 6-7). All MD thermal desorption profiles had peaks in the -N range, but the second common profile shape (sample b) had low concentrations and a large component of organic Hg compounds in addition to -N. All thermal desorption profiles are shown in Figure SI 7.

Sample a was characterized by a strong -N peak (69 % of peak) with -S (19%) and -Br/Cl (12%) compounds (Figure 2). Sample Figure 2 MD a, along with other profiles sharing this shape, had high % breakthrough (12%). This suggests, similar to GH results, that RM compounds collected on the nylon membrane when N-based have a lower capture efficiency than the other GOM compounds on the membranes. Trajectory points for this sample did not reside in any defined source boxes for significant times. During this sample deployment, the MD site was influenced by air travelling across the continental United States with air masses originating from the west and southwest (Figure 4 MD a) and 1%

within 100 km of the site. There was a high density of trajectories, > 50% of total (red), over Pennsylvania, Ohio, and West Virginia, areas with documented coal burning activity that release SO₂, NO_x, chlorine, and Hg¹⁶. The influence of coal burning near the area is reflected by the composition of the RM species on the membrane. The air flow pattern further supports that coal-fired power plant emissions influenced RM chemistry at MD.

323

324

325

326

327

328

329

330

331

332

333

334

335

336

337

338

339

340

341

342

343

The profile for Sample b was bimodal, with organic-Hg compounds (54%), -N (15%), -S (3%), and -Br/Cl (28%) compounds (Figure 2 MD b). The samples at this site with high organic-Hg were collected from May through July, 2018. Biogenic compounds, such as isoprene and nitrogen oxides, have been observed to be highest during the summer months in North America^{25,26}. Additionally, MD samples dominated by organic-Hg compounds had low breakthrough, 2% or less, for nylon membranes. In contrast, when -N compounds dominated, the breakthrough was high (see excel spreadsheet in the SI). When organic-Hg is present, regardless of the presence on -N on the sample, the breakthrough percentage was low indicating that organic-Hg compounds may enhance the sorption efficiency of the nylon membranes for -N compounds. Back trajectories showed air flow predominantly from the southeast over the Atlantic Ocean. Many of these trajectories were within the calculated marine boundary layer and then followed a path over land (Figure 4 MD b). Four % of the trajectory points were within 100 km of the site. IMPROVE data collected at this site (PRAAMS, MD08) showed that organic matter (hence organic compounds) and sulfate are the dominant compounds on the aerosols (data not shown), supporting our observations.

The MD nylon membrane RM concentrations were 31 to 85% lower than CEM RM concentrations for the entire campaign. The low efficiency of the nylon membranes relative to CEM is thought to be attributed to the predominance of -N compounds at MD. No MD samples were analyzed by IC.

3.4 UT

Mean RM concentration of all CEM collected at UT was 38 ± 4 pg m⁻³. Nylon membranes had a mean RM concentration of 19 ± 2 pg m⁻³ (Figure 1d). Mean breakthrough percentages for CEM and nylon membranes were $19 \pm 6\%$ and $9 \pm 4\%$, respectively.

UT sample 5a had a profile dominated by -Br/Cl compounds with a small peak at high temperature in the organic-Hg range (Figure 2 UT a). The air flow patterns were from the west. Total residence times for trajectory points during sample a deployment was 4.08% for the Northern Eurasian source box, 1.13% for East Asian source box, and 1.84% for San Francisco source box. Greater than 25% of trajectory points traveled below the marine boundary layer over the East Asian source box (Figure 5a). In this case, 6.9% of the trajectory points were within 100 km of the site.

Trajectories for sample UT b showed air passed over the Asian continent, Alaska, Canada, and the Pacific Ocean (Figure 4). A large percentage, 9.6%, of total trajectory points resided in the Northern Eurasia source box. and 1.0% of points resided in the East Asia source box. Some trajectories resided beneath the boundary layer over East Asia, with a heightened density of trajectories (yellow: 5-25%) and 2.2% of the trajectory points were

within 100 km of the site. For additional trajectories with ion chemistry see Figure SI 9 and all trajectories Figure SI 10.

Peak deconvolution proportions were 28% -0, 31% -Br/Cl, 39 % -N, and 3% organic-Hg compounds. Ninety-two % of ions detected by IC were SO₄²⁻ and 8% were NO₃⁻ (For additional ion concentrations see Table SI 4). The presence on SO₄²⁻ on the membrane does not correspond with peak deconvolution results, indicating that 1) -S compounds were not participating in the oxidation of GEM, 2) the compounds degraded in the air or on the membrane or 3- membranes were sorbing other S gases/particles that do not match our standard profile. Based on the evidence provided by peak deconvolution and back trajectories, RM chemistry was dominantly influenced by long-range transport from Asia. Long-range transport of Hg from Eurasia and Asia has been observed in other studies for the Western United States¹¹. In addition, elevated SO₄²⁻ was observed on IMPROVE network filters collected at Great Basin National Park associated with long-range transport from Eurasia and elevated O₃ events^{11,27}.

Thermal desorption profiles indicated the primary compounds were -Br/Cl and -N based in Winter 2017; -O, -Br/Cl, and -N compounds in Spring 2018; -Br/Cl and -O in Summer 2018; -O, -Br/Cl, -N, and -S in Fall 2018; and -O, -Br/Cl, -N, and -S compounds in winter 2018 (See profiles in SI). It is important to note that in Winter 2017 there were no multiday inversion episodes. More data and discussion will be presented in a future publication (Lyman et al., in prep).

Major implications

384

385

386

387

388

389

390

391

392

393

394

395

396

397

398

399

400

401

402

403

404

UNR-RMAS 2.0 CEM RM concentrations were higher than Tekran® RM concentrations in all cases, except for four 2-week periods given the error bars at MLO. Tekran® data exhibited similar temporal trends as CEM measurements, and in general were not well correlated (Table SI 4); and did not collect RM compounds as efficiently, and this varied by location. This is consistent with past studies comparing CEM and Tekran® RM concentrations^{3, 4, 7}. At the GH and MD sites that had more diverse thermal desorption profiles, the temporal trends between Tekran® and membranes measurements did not follow similar patterns and concentrations were low (< 6 pg m⁻³ on average for each deployment period for Tekran measurements). This reflects the lower efficiency of the KClcoated denuder to collect -S, -N, and organic-Hg RM compounds. It is noteworthy that the HgCl₂ was the form that was used for development of the KCl denuder²⁸ and good recovery rates were achieved with this compound. Thus, during the good agreement periods at MLO it is likely this reflect input from the marine boundary layer. It is noteworthy that this air would be humid and this indicates that the membranes are not specifically affected by RH. In addition, Gustin et al.⁵ found that absolute humidity had no influence on CEM concentrations. Absolute humidity is the density of water vapor in the air (kg m⁻³) and is independent of solar radiation.

All sites had lower RM concentrations on the nylon membranes than the CEM (Figure 1), except for GH during the summer of 2018 that were dominated by –Br/Cl-containing compounds. Thus, the CEM were more efficient at collecting total RM than nylon

membranes, but the ratio of nylon membrane RM concentrations to CEM concentrations varied for different RM compounds due to RM chemistry.

405

406

407

408

409

410

411

412

413

414

415

416

417

418

419

420

421

422

423

424

425

In order from lowest to highest, breakthrough was: MLO (CEM: 5 ± 1%, nylon: 1.2 ± 0.3%) < GH (CEM: 13 ± 1, nylon: 7 ± 2%) < MD (CEM: 15 ± 7%, nylon: 8 ± 3%) < UT (CEM: $19 \pm 6\%$, nylon: $9 \pm 4\%$). For the nylon membranes this is attributed to the presence of -N compounds. This may also be true for the other locations for the CEM, or other conditions could be influencing these membranes. Further work is needed to better understand the limitations of the membranes under a variety of conditions. For example, whether reactions are occurring on the membranes needs to be better understood. However, because CEM concentrations have been found to be similar to a calibrated dual channel system (Lyman et al. 15) the CEM is more accurate than the Tekran system. In addition, because membranes did not significantly lose ambient RM and thermal desorption profiles remained the same after holding for 6 months (Dunham-Cheatham et al. ²⁹) suggests membranes retain RM compounds. Limited work has demonstrated that the CEM retains HgCl₂ and HgBr₂ after being spiked and deployed ^{29, 30}. IC results in some cases agreed with the compounds determined based on thermal desorption profiles. However, at some locations SO₄²- was measured using IC and there were not -S based RM compounds detected in the thermal desorption profiles. This suggests that reactions were not occurring on the membranes forming -S compounds. The least common ion in the samples was Br-, that only made up 1% of the total ions when detected. It is possible that if there were bromine ions on the nylon membranes, they were not in the Br- form.

As noted, the exact compounds thermally desorbed from the nylon membranes are unknown. However, comparing thermal desorption behavior with that of pure standard compounds is a significant step forward in discerning RM chemistry.

This work demonstrated that the UNR-RMAS 2.0 provides a more quantitative measure of RM concentrations than the Tekran® system, and a step towards understanding of RM chemistry. The UNR-RMAS 2.0 membrane data paired with peak deconvolution, ion chromatography, back trajectories, and site air chemistry relationships revealed important information for understanding how RM concentrations and chemistry changed across space and time.

Deployment of the RMAS 2.0 at locations with a Tekran® 2537/1130/1135 system would provide a framework for better understanding of the discrepancy between more accurate RM concentrations versus those measured by the Tekran®. However, given that the chemistry of RM compounds depends on the oxidants in air and some RM compounds are more efficiently measured by the Tekran® (halogenated), correction of past Tekran® data will be a rough estimation.

Acknowledgements

Special thanks to Nash Kobayashi and Marty Martinsen for collecting and deploying our samplers on Mauna Loa. The authors also thank Peter Weiss-Penzias and Ashley Pierce for their instruction on HYSPLIT methods. Ion chromatography analyses were made possible through help from Riley Dunavent and Dr. Glenn Miller. We thank the Gustin lab undergraduates Margarita Vargas Estrada, Molly Willoughby, and Samir Gulati. We also thank the University of Nevada, Reno Department of Natural Resources and Environmental Science for providing support through a teaching assistantship. The authors thank the 3 anonymous reviewers for providing useful comments. This work was made possible by the National Science Foundation Atmospheric Chemistry Program Grant Numbers 629679 and 1700722. The scientific results and conclusions, as well as any views or opinions expressed

- herein, are those of the author(s) and do not necessarily reflect the views of NOAA or the
- 453 Department of Commerce.

454

- Supporting Information consists of two documents. One is an excel file containing the data
- 456 for all deployments. The second is 3 pages in length and includes 10 pgs of text, 4 tables,
- 457 and 10 figures.

458

References

459 460

- 461 1. Ariya, P. A.; Amyot, M.; Dastoor, A.; Deeds, D.; Feinberg, A.; Kos, G.; Poulain, A.; Ryjkov, A.;
- Semeniuk, K.; Subir, M.; Toyota, K., Mercury Physicochemical and Biogeochemical Transformation in the
- 463 Atmosphere and at Atmospheric Interfaces: A Review and Future Directions. *Chemical Reviews* **2015,**
- 464 115, (10), 3760-3802.
- 465 2. Miller, M. B.; Gustin, M. S., Gas-exchange chamber analysis of elemental mercury
- deposition/emission to alluvium, ore, and mine tailings. *Chemosphere* **2015**, *131*, 209-216.
- 467 3. Gustin, M. S.; Huang, J. Y.; Miller, M. B.; Peterson, C.; Jaffe, D. A.; Ambrose, J.; Finley, B. D.;
- Lyman, S. N.; Call, K.; Talbot, R.; Feddersen, D.; Mao, H. T.; Lindberg, S. E., Do We Understand What the
- 469 Mercury Speciation Instruments Are Actually Measuring? Results of RAMIX. *Environmental Science* &
- 470 *Technology* **2013,** 47, (13), 7295-7306.
- 471 4. Ambrose, J. L.; Lyman, S. N.; Huang, J. Y.; Gustin, M. S.; Jaffe, D. A., Fast Time Resolution
- 472 Oxidized Mercury Measurements during the Reno Atmospheric Mercury Intercomparison Experiment
- 473 (RAMIX). Environmental Science & Technology **2013**, 47, (13), 7285-7294.
- 474 5. Gustin, M.S., Dunham-Cheatham, S. M., Zhang, L. 2019 Comparison of 4 Methods
- for Measurement of Reactive Gaseous Oxidized, and Particulate Bound Mercury Environmental Science
- 476 and Technology, 53, 24, 14489-14495 DOI 10.1021/acs.est.9b04648
- 477 6. Huang, J. Y.; Gustin, M. S., Uncertainties of Gaseous Oxidized Mercury Measurements Using KCl-
- 478 Coated Denuders, Cation-Exchange Membranes, and Nylon Membranes: Humidity Influences.
- 479 Environmental Science & Technology **2015**, 49, (10), 6102-6108.
- 480 7. Huang, J. Y.; Miller, M. B.; Weiss-Penzias, P.; Gustin, M. S., Comparison of Gaseous Oxidized Hg
- 481 Measured by KCl-Coated Denuders, and Nylon and Cation Exchange Membranes. *Environmental Science*
- 482 & Technology **2013**, 47, (13), 7307-7316.
- 483 8. Talbot, R.; Mao, H. T.; Feddersen, D.; Smith, M.; Kim, S. Y.; Sive, B.; Haase, K.; Ambrose, J.; Zhou,
- 484 Y.; Russo, R., Comparison of Particulate Mercury Measured with Manual and Automated Methods.
- 485 *Atmosphere* **2011,** *2*, (1), 1-20.
- 486 9. Gustin, M. S.; Pierce, A. M.; Huang, J. Y.; Miller, M. B.; Holmes, H. A.; Loria-Salazar, S. M.,
- 487 Evidence for Different Reactive Hg Sources and Chemical Compounds at Adjacent Valley and High
- 488 Elevation Locations. Environmental Science & Technology 2016, 50, (22), 12225-12231.
- 489 10. Peterson, C.; Gustin, M.; Lyman, S., Atmospheric mercury concentrations and speciation
- 490 measured from 2004 to 2007 in Reno, Nevada, USA. Atmospheric Environment 2009, 43, (30), 4646-
- 491 4654.
- 492 11. Pierce, A. M.; Gustin, M. S.; Christensen, J. N.; Loria-Salazar, S. M., Use of multiple tools including
- lead isotopes to decipher sources of ozone and reactive mercury to urban and rural locations in Nevada,
- 494 USA. Science of the Total Environment **2018**, *615*, 1411-1427.

- 495 12. Huang, J. Y.; Miller, M. B.; Edgerton, E.; Gustin, M. S., Deciphering potential chemical
- compounds of gaseous oxidized mercury in Florida, USA. Atmospheric Chemistry and Physics 2017, 17,
- 497 (3), 1689-1698.
- 498 13. Miller, M.B.; Howard, D.A.; Pierce, A.M; Cook, K.; Keywood, M.; Gustin, M.S., Edwards, G.C.
- 499 Reactive mercury concentrations in Australia and the Southern Hemisphere submitted to STOTEN May
- 500 1 2020, in revision.

501

- 502 14. Luippold, A.; Gustin, M.; Dunham-Cheatham, S.; Zhang, L., Improvement of quantification and identification of atmospheric reactive mercury. *Atmospheric Environment* **2020**, *224*.
- 504 http://www.elsevier.com/locate/atmosenv https://doi.org/10.1016/j.atmosenv.2020.117307

505

506 15. Lyman, S.; Gratz, L.; Dunham-Cheatham, S.M.; Gustin, M. S.; Luippold, A. Improvements to the accuracy of atmospheric oxidized mercury measurements. Submitted to Environmental Science and Technology April 30, 2020

509

- 16. Castro, M. S.; Moore, C.; Sherwell, J.; Brooks, S. B., Dry deposition of gaseous oxidized mercury in Western Maryland. *Science of the Total Environment* **2012**, *417*, 232-240.
- 512 17. Castro, M. S.; Sherwell, J., Effectiveness of Emission Controls to Reduce the Atmospheric
- 513 Concentrations of Mercury. *Environmental Science & Technology* **2015**, *49*, (24), 14000-14007.
- 514 18. Cheng, I.; Zhang, L. M.; Castro, M.; Mao, H. T., Identifying Changes in Source Regions Impacting
- 515 Speciated Atmospheric Mercury at a Rural Site in the Eastern United States. *Journal of the Atmospheric*
- 516 Sciences **2017**, 74, (9), 2937-2947.
- 517 19. Lyman, S.; Tran, T., Inversion structure and winter ozone distribution in the Uintah Basin, Utah,
- 518 USA. *Atmospheric Environment* **2015**, *123*, 156-165.
- 519 20. Draxier, R. R.; Hess, G. D., An overview of the HYSPLIT_4 modelling system for trajectories,
- 520 dispersion and deposition. Australian Meteorological Magazine 1998, 47, (4), 295-308.
- 521 21. Stein, A. F.; Draxler, R. R.; Rolph, G. D.; Stunder, B. J. B.; Cohen, M. D.; Ngan, F., NOAA's
- 522 HYSPLIT Atmospheric Transport and Dispersion Modeling System. In 2015.
- 523 22. Neal, C. A.; Brantley, S. R.; Antolik, L.; Babb, J. L.; Burgess, M.; Calles, K.; Cappos, M.; Chang, J. C.;
- 524 Conway, S.; Desmither, L.; Dotray, P.; Elias, T.; Fukunaga, P.; Fuke, S.; Johanson, I. A.; Kamibayashi, K.;
- Kauahikaua, J.; Lee, R. L.; Pekalib, S.; Miklius, A.; Million, W.; Moniz, C. J.; Nadeau, P. A.; Okubo, P.;
- Parcheta, C.; Patrick, M. R.; Shiro, B.; Swanson, D. A.; Tollett, W.; Trusdell, F.; Younger, E. F.; Zoeller, M.
- 527 H.; Montgomery-Brown, E. K.; Anderson, K. R.; Poland, M. P.; Ball, J. L.; Bard, J.; Coombs, M.; Dietterich,
- 528 H. R.; Kern, C.; Thelen, W. A.; Cervelli, P. F.; Orr, T.; Houghton, B. F.; Ganseddi, C.; Hazlett, R.; Lundgren,
- 529 P.; Diefenbach, A. K.; Lerner, A. H.; Waite, G.; Kelly, P.; Clors, L.; Werner, C.; Mulliken, K.; Fisher, G.;
- 530 Damby, D., The 2018 rift eruption and summit collapse of Kilauea Volcano. Science 2019, 363, (6425),
- 531 367-+.
- 532 23. Lin, M. Y.; Horowitz, L. W.; Oltmans, S. J.; Fiore, A. M.; Fan, S. M., Tropospheric ozone trends at
- Mauna Loa Observatory tied to decadal climate variability. *Nature Geoscience* **2014,** 7, (2), 136-143.
- 534 24. Subir, M.; Ariya, P. A.; Dastoor, A. P. A review of the sources of uncertainties in
- atmospheric mercury modeling II. Mercury surface and heterogeneous chemistry A missing
- 536 link. Atmos. Environ. 2012, 46, 1–10.
- Rutter, A. P.; Schauer, J. J. The impact of aerosol composition on the particle to gas
- partitioning of reactive mercury. Environ. Sci. Technol. 2007, 41 (11), 3934–3939.

539 540 26. Marusczak, N.; Sonke, J. E.; Fu, X. W.; Jiskra, M., Tropospheric GOM at the Pic du Midi 541 Observatory-Correcting Bias in Denuder Based Observations. Environmental Science & Technology 2017, 542 51, (2), 863-869. 543 VanCuren, R.; Gustin, M. S., Identification of sources contributing to PM2.5 and ozone at 27. 544 elevated sites in the western US by receptor analysis: Lassen Volcanic National Park, California, and 545 Great Basin National Park, Nevada. Science of the Total Environment 2015, 530, 505-518. 546 547 28. Landis, M. S.; Stevens, R. K.; Schaedlich, F.; Prestbo, E. M., Development and characterization of 548 an annular denuder methodology for the measurement of divalent inorganic reactive gaseous mercury 549 in ambient air. Environmental Science & Technology 2002, 36, (13), 3000-3009. 550 29. Pierce, A.M.; Gustin, M. S. Development of a Particulate Mass Measurement System for 551 Quantification of Ambient Reactive Mercury. Environmental Science & Technology 2017; 51: 552 436-445. 553 554 30. Dunham-Cheatham, S.M.; Lyman, S.N.; Gustin, M.S. 555 Evaluation of sorption surface materials for reactive mercury compounds. Atmospheric Environment, 556 submitted April 2020 557 558 559 560

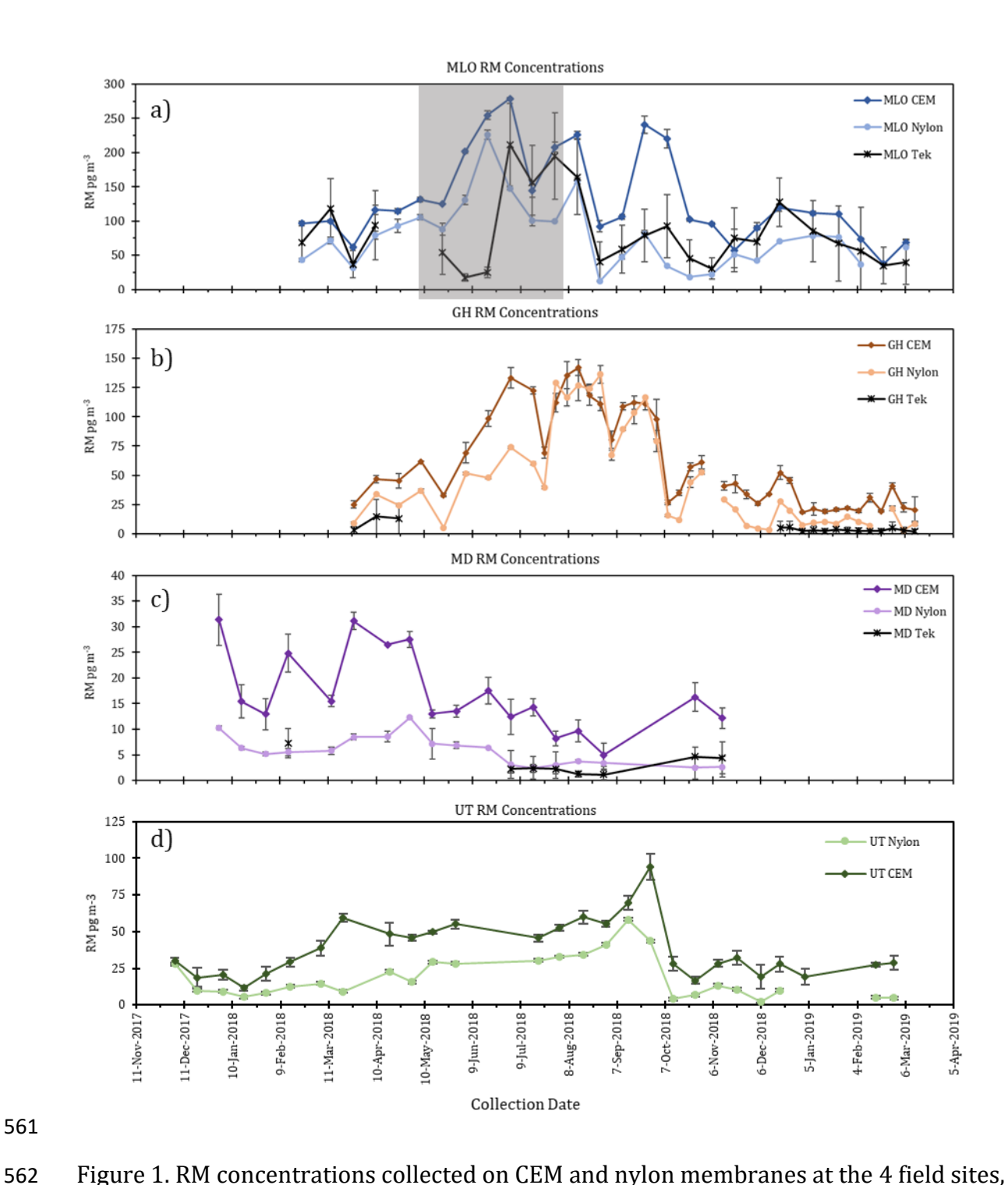


Figure 1. RM concentrations collected on CEM and nylon membranes at the 4 field sites, and Tekran® system RM concentrations (MLO 1130/1135/2537, GH 1130/2537, MD 1130/1135/2537). The grey box highlights the duration of the Kilauea volcanic eruption. Note differences of scale on y-axes. Error bars (1 σ) are shown where n \geq 3.

a) b) 12% **Kelego (M.)** 150 **(M.)** 150 **(M.)** 50 26% 78% 10% 180 33% a) b) 6% c) 31% 14% Hg Released (pg) 41% 22% 47% 35% 14% 28% 15% 3% 11% 12% 28% a) b) 15% 69% Hg Released (pg) 19% 3% ð 54% **Legend** 11% Black = average curve a) b) 28% 51% 31% Yellow = Br/Cl Hg Released (pg) 32% 39% Brown = Br/Cl/N 6% 3% Blue = 0Grev = N

Common Thermal Desorption Profiles From Each Site

Figure 2. Examples of the common desorption profile shapes from each field site. Black curves with black data points are the average thermal desorption profile from replicate (n = 3) nylon membranes. Curves without data points are the deconvoluted peaks of RM compounds, where yellow = -Br/Cl, brown = -Br/Cl/N, blue = -0, grey = -N, green = -S, and purple = organic-Hg. Percentages represent relative amounts of RM compounds in each sample compared to the total RM. The profiles from each site are labelled alphabetically to correspond with the back trajectories shown in Figures 3 and 4.

Temperature (°C)

 Temperature (°C)

Green = S

Purple = Organic-Hg

Mauna Loa Observatory (MLO) Back Trajectories

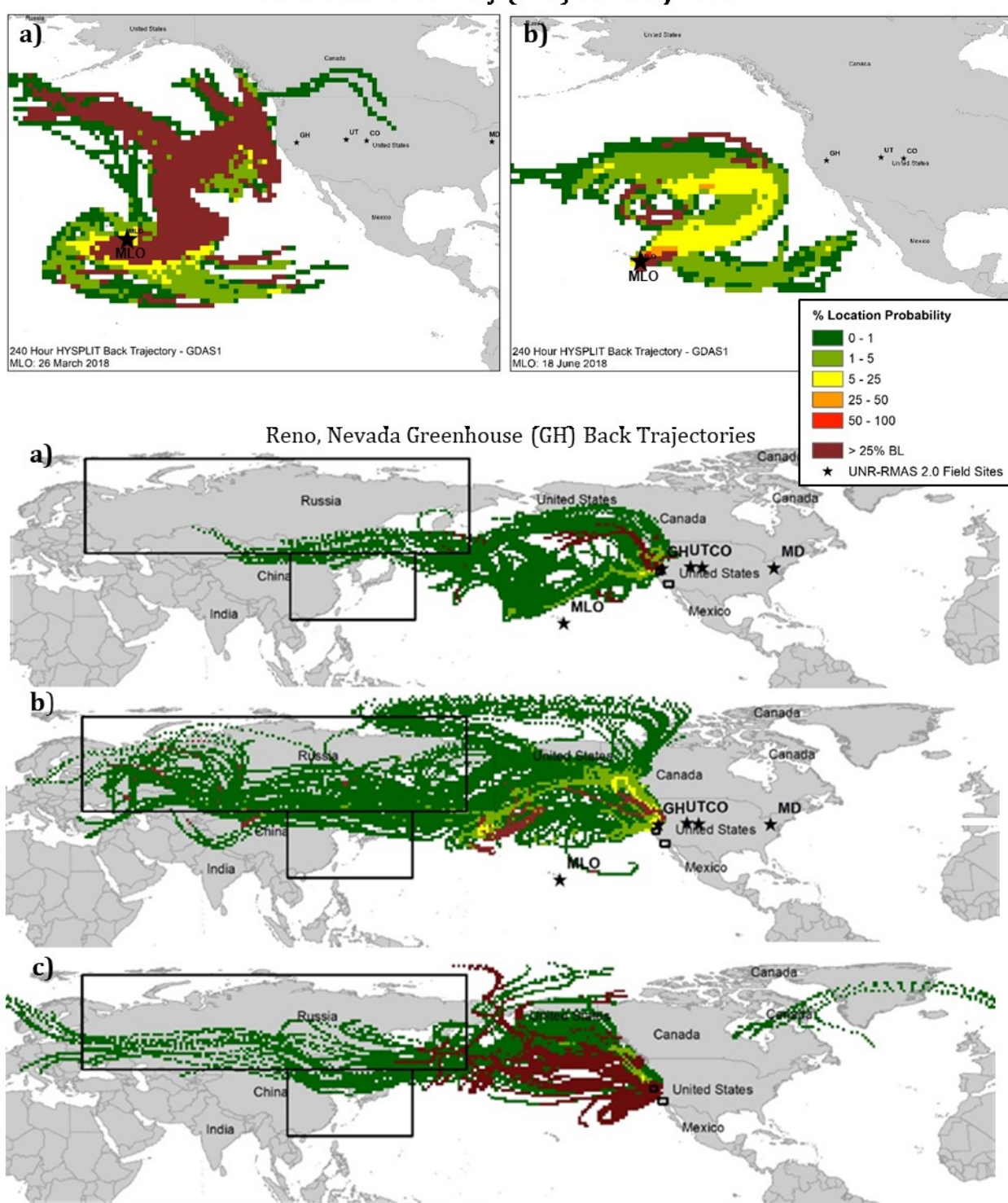
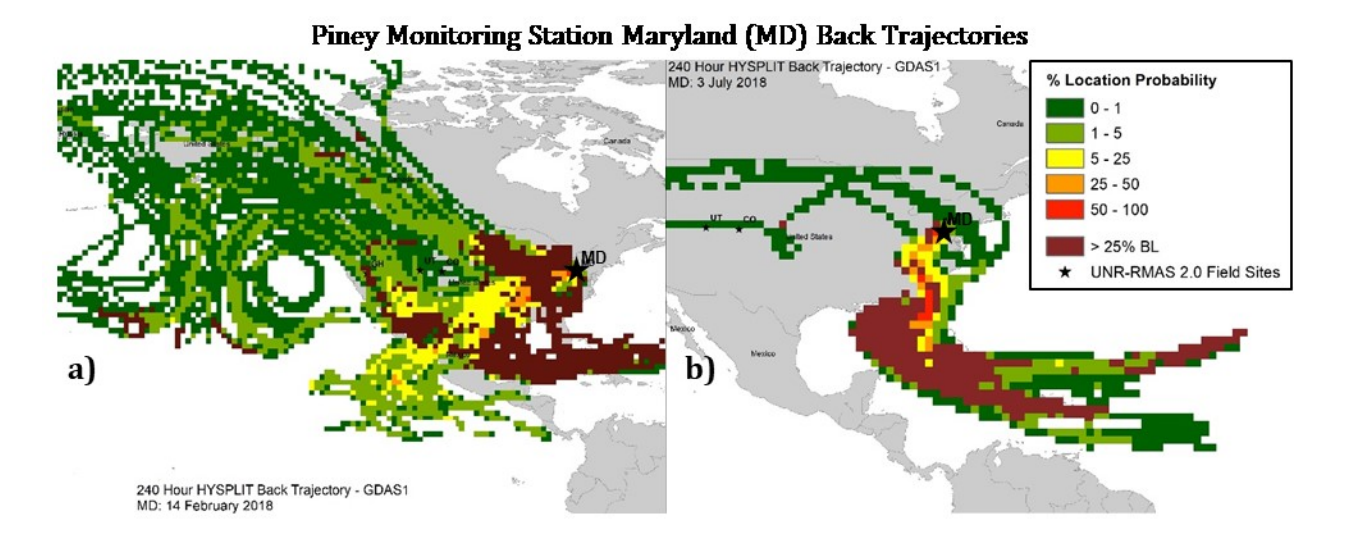


Figure 3. 10-day back-trajectory point frequency distributions are shown for MLO and GH sites. Brown indicates grids where > 25% of trajectories in that grid were within the marine boundary layer. The alphabetical labels correspond to the MLO and GH thermal desorption profiles in Figure 2.



Horsepool Monitoring Station, Utah (UT) Back Trajectories

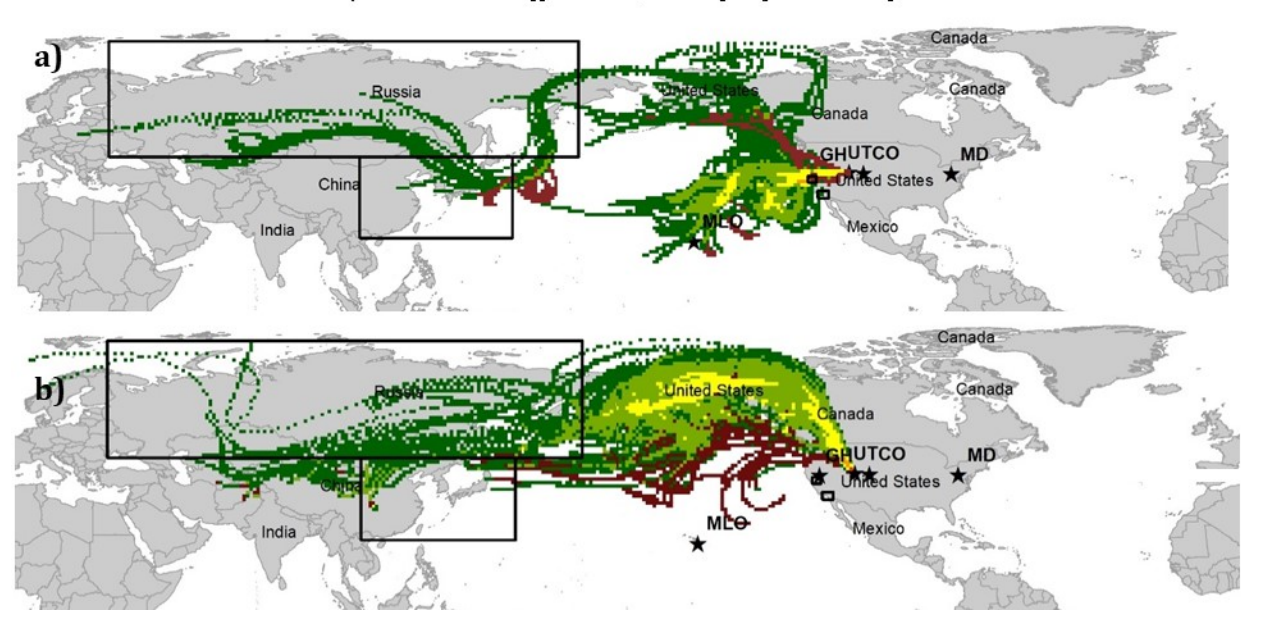


Figure 4. 10-day back-trajectory point frequency distributions are shown for MD and UT sites. Brown indicates grids where > 25% of trajectories in that grid were within the marine boundary layer. The alphabetical labels correspond to the MD and UT thermal desorption profiles in Figure 2.